Observation of $\pi/2$ Modes in an Acoustic Floquet System

Zheyu Cheng,[1] Raditya Weda Bomantara,[2,3] Haoran Xue,[1] Weiwei Zhu,[4] Jiangbin Gong,[4,5,*] and Baile Zhang[1,6,†]

[1]*Division of Physics and Applied Physics, School of Physical and Mathematical Sciences, Nanyang Technological University, Singapore 637371, Singapore*

[2]*Centre for Engineered Quantum Systems, School of Physics, University of Sydney, Sydney, New South Wales 2006, Australia*

[3]*Department of Physics, King Fahd University of Petroleum and Minerals, 31261 Dhahran, Saudi Arabia*

[4]*Department of Physics, National University of Singapore, Singapore 117542, Singapore*

[5]*Centre for Quantum Technologies, National University of Singapore, 117543 Singapore*

[6]*Centre for Disruptive Photonic Technologies, Nanyang Technological University, Singapore 637371, Singapore*

(Received 21 July 2022; accepted 8 November 2022; published 16 December 2022)

Topological phases of matter have remained an active area of research in the last few decades. Periodic driving is a powerful tool for enriching such exotic phases, leading to various phenomena with no static analogs. One such phenomenon is the emergence of the elusive $\pi/2$ modes, i.e., a type of topological boundary state pinned at a quarter of the driving frequency. The latter may lead to the formation of Floquet parafermions in the presence of interaction, which is known to support more computational power than Majorana particles. In this Letter, we experimentally verify the signature of $\pi/2$ modes in an acoustic waveguide array, which is designed to simulate a square-root periodically driven Su-Schrieffer-Heeger model. This is accomplished by confirming the $4T$-periodicity (T being the driving period) profile of an initial-boundary excitation, which we also show theoretically to be the smoking gun evidence of $\pi/2$ modes. Our findings are expected to motivate further studies of $\pi/2$ modes in quantum systems for potential technological applications.

DOI: 10.1103/PhysRevLett.129.254301

Introduction.—Topology plays a significant role in condensed matter physics through its ability to protect certain physical properties against perturbations. Its presence has been identified in a variety of systems including topological insulators [1,2], topological semimetals [3,4], and topological superconductors [5,6]. These topological phases share one defining feature, i.e., they support robust boundary modes protected by a global quantity, i.e., the topological invariant.

Since the last decade, the implementation of periodic driving in studies of topological phases has been extensively pursued [7–25]. Not only does periodic driving have the capability to turn an otherwise normal system into a topological one [7–9], but it can also generate unique topological features with no static counterparts [19–26]. The latter is made possible by the periodicity nature of quasienergy, i.e., the analog of energy in time-periodic systems. It prominently includes the coexistence of boundary zero and π modes, respectively pinned at quasienergy of zero and half the driving frequency. Such a feature has recently been exploited for quantum computing applications [27–30].

Periodically driven (hereafter referred to as Floquet) systems can support even richer topological features beyond the above zero and π modes. The so-called $\pi/2$ modes are of particular interest, i.e., boundary modes pinned at a quarter of the driving frequency. They were first theoretically proposed in [31] as edge modes arising in a chain of periodically driven parafermions. By contrast, π modes were first theoretically proposed in [25] as edge modes arising in a chain of periodically driven Majorana fermions. Since parafermion modes are known to support richer topologically protected quantum gate operations than their Majorana counterparts [32], such $\pi/2$ modes emerge as the more attractive variants of the more common π modes. On the other hand, while π modes have been previously observed [16,23], to our knowledge, $\pi/2$ modes have not been experimentally confirmed. That the $\pi/2$ mode was proposed either in a very elaborate driven system [22] or in a strongly interacting system [31] contributes to the difficulty in experimentally realizing them.

In this Letter, we adapt the theoretical square-root procedure of Refs. [33,34] to construct an experimentally feasible Floquet system capable of supporting the elusive $\pi/2$ modes, along with zero and π modes simultaneously. We then adopt the experimental technique of Ref. [23] to realize such a system in acoustic waveguides and subsequently detect $\pi/2$ modes. To this end, we theoretically show and experimentally verify that a state injected at one end of the system displays a $4T$ periodicity when zero, π, and $\pi/2$ modes coexist. Our experiments not only confirm the existence of $\pi/2$ modes but also capture their signature when zero and π modes are additionally present.

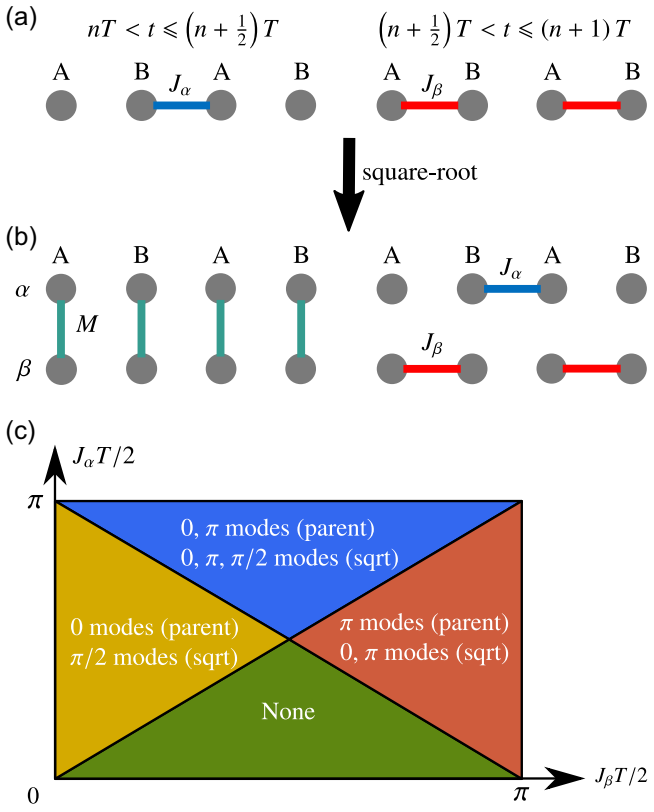

FIG. 1. Schematic of (a) Floquet SSH model and (b) its square-root counterpart. (c) Phase diagram for square-root and parent Floquet system.

Square-root Floquet SSH model.—We consider a system of two one-dimensional (1D) chains subjected to the two-time-step Hamiltonian

$$H^{\mathrm{root}}(t) = \begin{cases} h_1^{\mathrm{root}} & nT < t \leq (n+\frac{1}{2})T \\ h_2^{\mathrm{root}} & (n+\frac{1}{2})T < t \leq (n+1)T \end{cases}, \tag{1}$$

where

$$h_1^{\mathrm{root}} = \sum_{j=1}^{N} \sum_{S=A,B} M|j,S,\alpha\rangle\langle j,S,\beta| + \mathrm{H.c.}, \tag{2}$$

$$h_2^{\mathrm{root}} = \sum_{j=1}^{N-1} J_\alpha|j,B,\alpha\rangle\langle j+1,A,\alpha| + \sum_{j=1}^{N} J_\beta|j,A,\beta\rangle\langle j,B,\beta| + \mathrm{H.c.} \tag{3}$$

$|j,S,\xi\rangle$ denotes a state at sublattice $S = A, B$ of the jth site in the chain species $\xi = \alpha, \beta$, and $n \in \mathbb{Z}$. It is schematically shown in Fig. 1(b) and can be understood as a nontrivial square root of a Floquet Su-Schrieffer-Heeger (SSH) model [see Fig. 1(a)]. Specifically, the parent model describes a system of *a single* 1D chain subjected to a two-time-step Hamiltonian of the form Eq. (1), such that during the first and second half of the period, it is respectively given by

$$h_1^{\mathrm{parent}} = \sum_{j=1}^{N-1} J_\alpha|j,B\rangle\langle j+1,A| + \mathrm{H.c.}, \tag{4}$$

$$h_2^{\mathrm{parent}} = \sum_{j=1}^{N} J_\beta|j,A\rangle\langle j,B| + \mathrm{H.c.} \tag{5}$$

The associated one-period time-evolution operator (hereafter referred to as the Floquet operator) is then given by

$$U^{\mathrm{parent}} = U_2^{\mathrm{parent}} U_1^{\mathrm{parent}}, \quad \text{where } U_j^{\mathrm{parent}} = \exp\left(-\mathrm{i}h_j^{\mathrm{parent}}\frac{T}{2}\right). \tag{6}$$

The use of an additional chain in our square-root model then introduces an ancillary degree of freedom that facilitates the square-rooting procedure [33] in the spirit of obtaining the Dirac equation [35] from the Klein-Gordon equation [36,37] (see also Ref. [38], as well as related theoretical [39–52] and experimental [53–56] studies).

Equation (1) can be intuitively understood as follows. A particle initially living in chain α (β) evolves under h_1^{parent} (h_2^{parent}) for the first half of the period and hops to the other chain in the second half of the period. The particle, which is now in chain β (α), then evolves under h_2^{parent} (h_1^{parent}) for another half period and hops back to the original chain α (β) at the end of the second period. Therefore, the particle effectively evolves one full period under the parent Hamiltonian when viewed over two periods. On the other hand, the particle undergoes a generally nontrivial evolution over one period that can give rise to new physics, including $\pi/2$ modes, the main focus of this Letter.

Mathematically, at $MT = (2m+1)\pi$ with $m \in \mathbb{Z}$, the Floquet operator associated with Eq. (1) can be easily obtained as

$$U^{\mathrm{root}} = \exp\left[-ih_2^{\mathrm{root}}\frac{T}{2}\right]\exp\left[-ih_1^{\mathrm{root}}\frac{T}{2}\right] = \begin{pmatrix} 0 & -iU_1^{\mathrm{parent}} \\ -iU_2^{\mathrm{parent}} & 0 \end{pmatrix}. \tag{7}$$

Indeed, up to a unitary transformation, U^{parent} is reproduced by $(U^{\mathrm{root}})^2 = -\mathrm{diag}(U_1^{\mathrm{parent}}U_2^{\mathrm{parent}}, U_2^{\mathrm{parent}}U_1^{\mathrm{parent}})$, as expected from our intuition above. As MT deviates from $(2m+1)\pi$, $(U^{\mathrm{root}})^2$ is no longer diagonal and directly related to U^{parent}. However, owing to the robustness of Floquet phases and as numerically demonstrated in

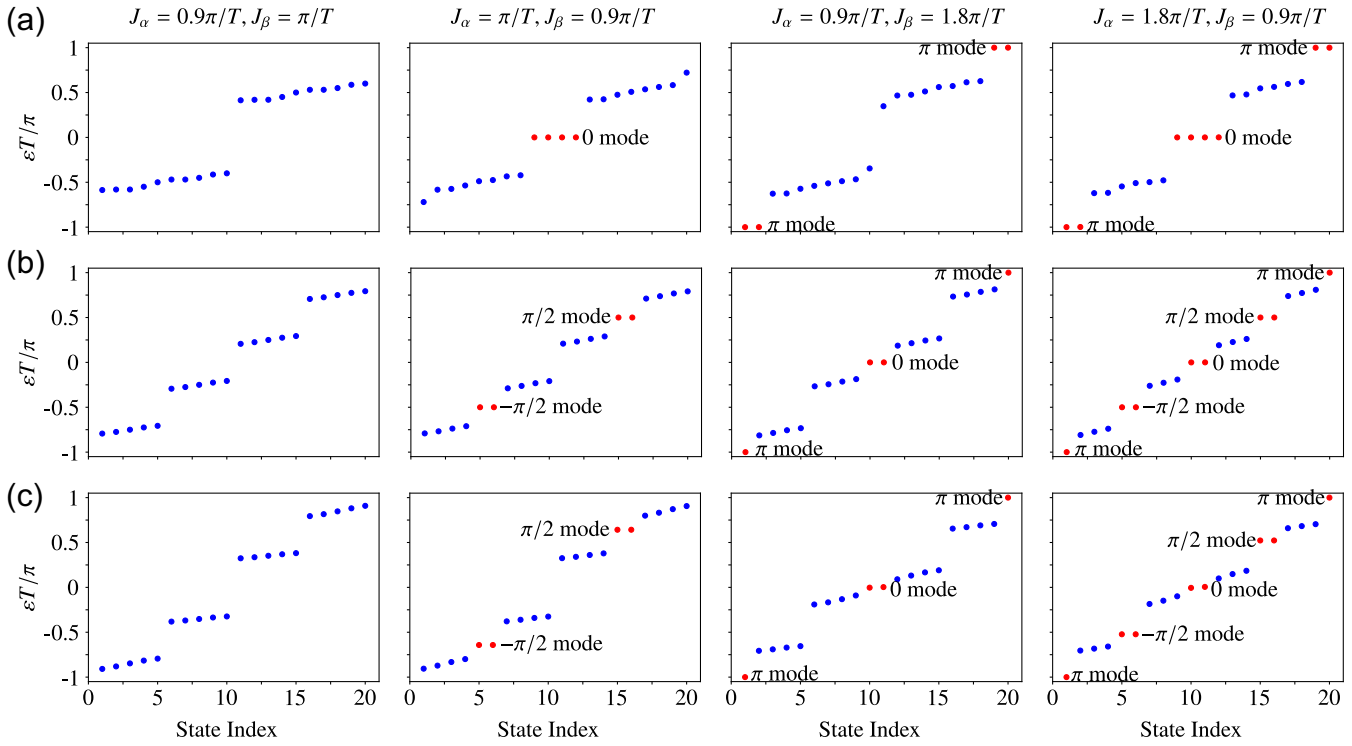

FIG. 2. (a) Illustration of quasienergy spectrum for two decoupled copies of parent Floquet system, each containing 10 sites. From left to right: $J_\alpha = 0.9\pi/T$, $J_\beta = \pi/T$; $J_\alpha = \pi/T$, $J_\beta = 0.9\pi/T$; $J_\alpha = 0.9\pi/T$, $J_\beta = 1.8\pi/T$; $J_\alpha = 1.8\pi/T$, and $J_\beta = 0.9\pi/T$. (b) and (c) Illustration of the quasienergy spectrum for a square-root Floquet system with 20 sites under (b) $M = \pi/T$, (c) $M = 1.3\pi/T$, and the same parameters J_α and J_β as panel (a).

Ref. [33], $(U^{\text{root}})^2$ still exhibits the physics expected from its parent system provided $MT - (2m+1)\pi$ is not too large.

Depending on the system parameter values, the parent Floquet SSH model may support either a pair of zero modes only, a pair of π modes only, a pair of zero modes and a pair of π modes, or neither of zero modes nor π modes. Here, 0 (π) modes are defined as the eigenstates of U^{parent} with eigenvalue 1 (-1). As elucidated in Ref. [33], the presence of π modes in the parent system leads to the coexistence of zero modes and π modes in its square-root counterpart, whereas the presence of zero modes in the former leads to the emergence of the elusive $\pi/2$ modes in the latter. Consequently, the proposed square-root Floquet SSH model possesses the phase diagram shown in Fig. 1(c) (see Supplemental Material [57] for its derivation).

Topological edge modes.—In Figs. 2(a)–2(c), we numerically calculate the quasienergy spectrum of the Floquet SSH model and its square-root counterpart at a representative point from each of the four phases in Fig. 1(c). There, in-gap quasienergy solutions at 0, $\pm\pi/T$, and $\pm\pi/(2T)$ correspond to zero, π, and $\pi/2$ modes, respectively, whose edge-localization nature is confirmed in Figs. 2(b) and 2(c) and the Supplemental Material. Figure 2(c) further verifies the robustness of zero, π, and $\pi/2$ modes in the square-root model against imperfection in the parameter M. There, all modes remain gapped from the rest of the bulk spectrum, with zero and π modes additionally remaining exactly pinned 0 and π/T quasienergy, respectively, whereas $\pi/2$ modes are slightly shifted away from $\pm\pi/(2T)$ quasienergy.

The quasienergy rigidity of the system's zero and π modes originates from the presence of chiral symmetry inherited from its parent model. Indeed, by writing the system's Floquet operator in the momentum space and under the symmetric time frame [60,61], i.e., the shift of time origin to $t_0 = T/4$, we obtain

$$\mathcal{U}^{\text{root}}(k) = e^{-i\mathcal{H}_1^{\text{root}}(k)\frac{T}{4}} e^{-i\mathcal{H}_2^{\text{root}}(k)\frac{T}{2}} e^{-i\mathcal{H}_1^{\text{root}}(k)\frac{T}{4}}, \tag{8}$$

where

$$\mathcal{H}_2^{\text{root}}(k) = J_\alpha \frac{\tau_0+\tau_3}{2}(\cos k\sigma_1 + \sin k\sigma_2) + J_\beta \frac{\tau_0-\tau_3}{2}\sigma_1,$$
$$\mathcal{H}_1^{\text{root}}(k) = M\tau_1\sigma_0, \tag{9}$$

$\tau_{1/2/3}$ and $\sigma_{1/2/3}$ are Pauli matrices acting on the chain species and sublattice subspace, respectively, and k is the quasimomentum. It can then be verified that $\mathcal{C}\mathcal{U}^{\text{root}}(k)\mathcal{C}^\dagger = [\mathcal{U}^{\text{root}}(k)]^\dagger$, where $\mathcal{C} = \tau_3\sigma_3$ is the chiral symmetry operator. As a result, the system's quasienergies come in pairs of ε and $-\varepsilon$. Moreover, the special values $\varepsilon = 0$ and $\varepsilon = \pi/T$ are at least twofold degenerate and can be chosen to be

simultaneous ± 1 eigenvalues of $\mathcal{C}$. The discreteness of $\mathcal{C}$ eigenvalues in turn protects the resulting degenerate eigenstates, i.e., zero and π modes, respectively.

At $MT = (2m+1)\pi$, there exists an additional subchiral symmetry that operates as $\mathcal{C}_{(1/2)}\mathcal{U}^{\mathrm{root}}(k)\mathcal{C}^{\dagger}_{(1/2)} = -\mathcal{U}^{\mathrm{root}}(k)$, where $\mathcal{C}_{(1/2)} = \tau_3\sigma_0$ [34,62]. It guarantees that the quasienergies of $\mathcal{U}^{\mathrm{root}}(k)$ come in pairs of ε and $\varepsilon \pm \pi/T$. Consequently, the special values $\varepsilon = \pm\pi/(2T)$ are at least twofold degenerate and can be chosen as simultaneous ± 1 eigenvalues of $\mathcal{C}\mathcal{C}_{(1/2)}$. The discreteness of $\mathcal{C}\mathcal{C}_{(1/2)}$ eigenvalues then protects the resulting $\pi/2$ modes. Such a subchiral symmetry no longer exists at $MT \neq (2m+1)\pi$, thus allowing $\pi/2$ modes to generally deviate from their expected $\pm\pi/(2T)$ quasienergy values. However, as demonstrated in the Supplemental Material, at small $\epsilon \equiv |MT - (2m+1)\pi|$, the shift in the quasienergy of the $\pi/2$ modes in the blue regime of Fig. 1 is at least second order in ϵ. This, coupled with the fact that their eigenmodes profile is similar to the ideal $MT = (2m+1)\pi$ case, justifies the term $\pi/2$ modes even as the $MT = (2m+1)\pi$ condition cannot be exactly achieved in our experiments.

The coexistence of zero, $\pm\pi/2$, and π modes, i.e., in the blue regime of Fig. 1(c), leads to a dynamical signature that we manage to observe in our experiment. In particular, by noting that $U^{\mathrm{root}}|0\rangle = |0\rangle$, $U^{\mathrm{root}}|\pm\pi/2\rangle = \mp\mathrm{i}|\pm\pi/2\rangle$, $U^{\mathrm{root}}|\pi\rangle = -|\pi\rangle$, for zero, $\pm\pi/2$, and π modes respectively, any superposition $|\psi\rangle = a|0\rangle + b|\pi/2\rangle + c|\pi\rangle + d|-\pi/2\rangle$ yields $4T$ periodicity. Indeed, throughout the period, each component of $|\psi\rangle$ acquires a relative phase of $\pi/2$, thus transforming it into a distinct state. After four periods, such a relative phase accumulates into 2π, thus recovering the state $|\psi\rangle$. On the other hand, in the absence of $\pm\pi/2$ modes, i.e., the orange regime of Fig. 1(c), the remaining coexistence of zero and π modes can similarly be probed by the $2T$-periodicity signature of a state comprising a superposition of $|0\rangle$ and $|\pi\rangle$.

Experimental realization in acoustic waveguides.—We will now present our experimental observation of $\pi/2$ modes in an acoustic waveguide array. To facilitate the theoretical description of our experiment, we consider the slowly varying amplitude (SVA) approximation $|(\partial^2 p)/(\partial z^2)| \ll k_z|(\partial p)/(\partial z)|$ and take $p \to pe^{ik_z z}$ to the Helmholtz equation $(\nabla^2 + \mathbf{k}^2)p = 0$, where p is the acoustic pressure. After SVA approximation, we get the paraxial wave equation, which can be written in the Schrödinger form

$$i\frac{\partial p}{\partial z} = H_{\mathrm{eff}}p = \left(-\frac{\nabla_\perp^2}{2k_z} - \frac{\mathbf{k}^2 - k_z^2}{2k_z}\right)p, \tag{10}$$

with $\nabla_\perp^2 = \partial_x^2 + \partial_y^2$ as the 2D Laplacian operator. By further employing a tight-binding approximation, Eq. (10) can then simulate the lattice model of Eq. (1) with tunable hopping amplitudes (see Supplemental Material). Here, "time" is simulated by "propagation direction" z. This scheme is the "paraxial acoustics," which is analogous to the "paraxial photonics" [63–66]. By periodically modulating the shape of the waveguides along the z direction, a Floquet system can be simulated. In this case, the wave function dynamics can be probed by detecting the pressure in the z direction.

To realize the acoustic analogy of Eq. (1), we construct the acoustic waveguide array (or 2D resonator system) as shown in Figs. 3(a)–3(c). The whole structure is covered by hard walls and filled with the air of density 1.8 $\mathrm{kg/m^3}$ and sound velocity 347 m/s. The length of one Floquet period is $L = 133$ mm, and eight Floquet periods are used in the simulation and experiment. In this setup, the waveguides (2D resonators) and link tubes simulate the lattice sites and nearest-neighboring hopping, respectively. As detailed in the Supplemental Material, the geometry of waveguides and the number of link tubes between two adjacent waveguides determine the hopping strength [J_α, J_β, M in Eq. (1)], respectively. Here, for example, $J_\alpha = 0.850\pi/T$ can be satisfied by six link tubes at 8 kHz, where T is the Floquet period in acoustic structure. The cross profile of the waveguide is a square with a side length $a = 10$ mm. The height and width of the coupling tubes are a and the length is $w = 5$ mm [see Fig. 3(a)]. To better simulate the "time" dimension from a "spatial" one, radiation boundary conditions at $z = 0$ and $z = 8L$ are chosen in our simulation to suppress the reflection. In the experiment, acoustic absorbing materials are inserted at $z = 0$ and $z = 8L$ to absorb acoustic waves impinging on them. Furthermore, we choose 8 kHz as the working frequency to reduce the reflection from coupling tubes (see Supplemental Material for details). After these implementations, the sound waves propagate along the $+z$ direction with negligible reflection, effectively behaving like time evolution.

We fabricated two experimental samples with different effective parameter values via 3D printing technology. For each sample, we drill 780 identical and equally spaced holes, inside which a microphone is inserted and responds to pressure [see Fig. 3(c)]. When not in use, these holes are covered by plugs. To numerically verify the dynamical signature of the $\pi/2$ edge modes, a speaker is placed at $z = 0$ on the lower-right corner [indicated by a red arrow in Fig. 3(b)], which generates an initial state $|1, A, \alpha\rangle$. While such a state might in principle still have nonzero overlap with the bulk modes, it is negligibly small as compared with the overlap with the boundary modes. In this case, the dynamics of such excitation are dominated by its boundary mode constituents. Moreover, as detailed in the Supplemental Material, it is approximately $\propto |0\rangle + |\pi/2\rangle + |\pi\rangle - |-\pi/2\rangle$ or $\propto |0\rangle + |\pi\rangle$ at the system parameters considered in our experiment, thus resulting in a clear $4T$-periodic or $2T$-periodic profile, respectively.

By measuring the acoustic pressure on the sample at some specific z values, the stroboscopic time evolution profile of the effective square-root Floquet SSH model can

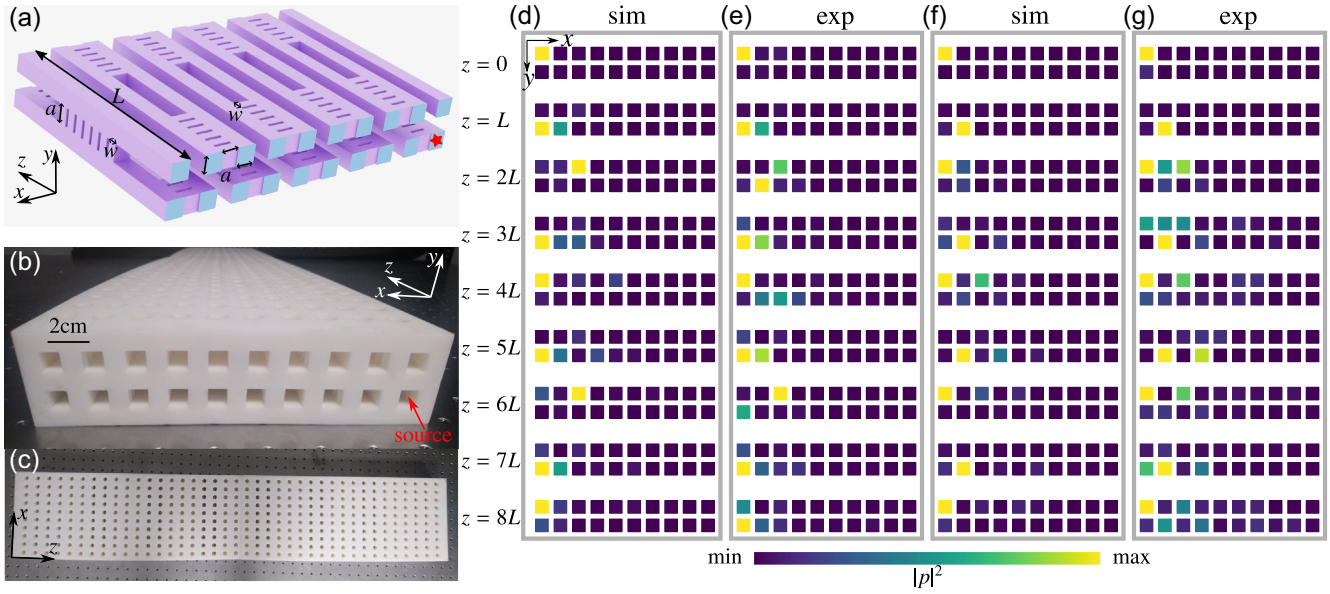

FIG. 3. (a) One Floquet period in the waveguide array, which hosts $0, \pi/2, \pi$ modes. An initial excitation was put at the red star in the simulation. The purple color is the hard boundary, and the light blue represents the air-filled hollow region. (b) and (c) Photo of the fabricated sample with plugs removed. The source was put in the lower-right corner in the measurement. (d) and (f) Mode evolution of full-wave simulation with $0, \pi/2, \pi(0, \pi)$ modes appear at 8 kHz accordingly. (e) and (g) Experimental counterparts of panels (d) and (f), respectively. The effective parameter values for the simulation and experimental results are (d),(e) $J_\alpha = 1.668\pi/T$, $J_\beta = 0.850\pi/T$, $M = 0.976\pi/T$ and (f),(g). $J_\alpha = 0.850\pi/T$, $J_\beta = 1.668\pi/T$, $M = 0.976\pi/T$.

be probed. A broadband sound signal is used, and Fourier transformation is performed to get 8 kHz field distribution. Our experimental results are summarized in Figs. 3(e) and 3(g), which are according to the blue and orange regime of Fig. 1(c), respectively. There, we only considered eight Floquet cycles for the following two reasons. First, due to the presence of loss in the experiment, the signal becomes weaker after a long evolution, thus making it harder to extract the corresponding mode profile. Second, consistent with our full-wave simulation [Figs. 3(d) and 3(f)], the presence and absence of $\pi/2$ modes already manifest themselves in the clear $4T$- and $2T$-period behavior of Figs. 3(e) and 3(g) respectively. Therefore, prolonging the number of Floquet cycles will not yield new information.

Concluding remarks.—In this Letter, we have proposed and experimentally realized a square-root Floquet SSH model, which exhibits "$\pi/(2T)$ quasienergy edge states" termed the $\pi/2$ modes, in coexistence with the more common zero and π modes. These exotic $\pi/2$ modes originate from the zero modes in the parent system and can thus be predicted by the topological invariant characterizing the latter, i.e., ν_0 as defined in the Supplemental Material. We have further identified a subchiral symmetry that protects these $\pi/2$ modes, as well as their dynamical signature, both of which enable their successful observation in our acoustic experiment.

Recently, Floquet topological systems which support coexisting zero and π modes were shown to be advantageous for quantum computation [28–30]. Moreover, the experimentally verified $\pi/2$ modes have been identified as the building blocks of the more attractive Z_4 parafermions [22]. The realization of coexisting zero, $\pi/2$, and π modes reported in this Letter thus opens up exciting opportunities for superior topological quantum computing beyond Majorana particles. These opportunities are further amplified by the fact that the present setup could be straightforwardly generalized to obtain other fractional $2\pi/k$ edge modes (see Supplemental Material for detail). Indeed, noting that many recent studies on the quantum computational aspects of Majorana fermions are motivated by the experimental signature of Majorana zero and π modes, it is expected that our results shall similarly stimulate similar studies on parafermions. While the present experiment concerns a classical system, it is expected that some of our findings can be carried over to the quantum realm. To this end, the simulation of braiding among the various edge modes we observed in our acoustic setup, e.g., achieved by adapting the technique of Ref. [67], may present a promising future direction.

Z. C., H. X., and B. Z. are supported by the Singapore Ministry of Education Academic Research Fund Tier 2 Grant No. MOE2019-T2-2-085, and Singapore National Research Foundation Competitive Research Program Grant No. NRF-CRP23-2019-0007. R. W. B. is supported by the Australian Research Council Centre of Excellence for Engineered Quantum Systems (EQUS, CE170100009).

W. Z. and J. G. are funded by the Singapore National Research Foundation Grant No. NRF-NRFI2017-04 (WBS No. R-144-000-378-281).

Z. C. and R. W. B. contributed equally to this work.

*phygj@nus.edu.sg
†blzhang@ntu.edu.sg

[1] B. A. Bernevig, T. L. Hughes, and S.-C. Zhang, Quantum spin Hall effect and topological phase transition in HgTe quantum wells, Science **314**, 1757 (2006).
[2] X.-L. Qi, T. L. Hughes, and S.-C. Zhang, Topological field theory of time-reversal invariant insulators, Phys. Rev. B **78**, 195424 (2008).
[3] A. A. Burkov and L. Balents, Weyl Semimetal in a Topological Insulator Multilayer, Phys. Rev. Lett. **107**, 127205 (2011).
[4] X. Wan, A. M. Turner, A. Vishwanath, and S. Y. Savrasov, Topological semimetal and Fermi-arc surface states in the electronic structure of pyrochlore iridates, Phys. Rev. B **83**, 205101 (2011).
[5] M. Z. Hasan and C. L. Kane, Colloquium: Topological insulators, Rev. Mod. Phys. **82**, 3045 (2010).
[6] X.-L. Qi and S.-C. Zhang, Topological insulators and superconductors, Rev. Mod. Phys. **83**, 1057 (2011).
[7] T. Oka and H. Aoki, Photovoltaic Hall effect in graphene, Phys. Rev. B **79**, 081406(R) (2009).
[8] T. Kitagawa, E. Berg, M. Rudner, and E. Demler, Topological characterization of periodically driven quantum systems, Phys. Rev. B **82**, 235114 (2010).
[9] N. H. Lindner, G. Refael, and V. Galitski, Floquet topological insulator in semiconductor quantum wells, Nat. Phys. **7**, 490 (2011).
[10] D. Y. H. Ho and J. Gong, Quantized Adiabatic Transport in Momentum Space, Phys. Rev. Lett. **109**, 010601 (2012).
[11] T. Kitagawa, M. A. Broome, A. Fedrizzi, M. S. Rudner, E. Berg, I. Kassal, A. Aspuru-Guzik, E. Demler, and A. G. White, Observation of topologically protected bound states in photonic quantum walks, Nat. Commun. **3**, 882 (2012).
[12] M. C. Rechtsman, J. M. Zeuner, Y. Plotnik, Y. Lumer, D. Podolsky, F. Dreisow, S. Nolte, M. Segev, and A. Szameit, Photonic Floquet topological insulators, Nature (London) **496**, 196 (2013).
[13] G. Jotzu, M. Messer, R. Desbuquois, M. Lebrat, T. Uehlinger, D. Greif, and T. Esslinger, Experimental realization of the topological Haldane model with ultracold fermions, Nature (London) **515**, 237 (2014).
[14] D. Y. H. Ho and J. Gong, Topological effects in chiral symmetric driven systems, Phys. Rev. B **90**, 195419 (2014).
[15] R. W. Bomantara and J. Gong, Generating controllable type-II Weyl points via periodic driving, Phys. Rev. B **94**, 235447 (2016).
[16] Q. Cheng, Y. Pan, H. Wang, C. Zhang, D. Yu, A. Gover, H. Zhang, T. Li, L. Zhou, and S. Zhu, Observation of Anomalous π Modes in Photonic Floquet Engineering, Phys. Rev. Lett. **122**, 173901 (2019).
[17] Y. Long and J. Ren, Floquet topological acoustic resonators and acoustic Thouless pumping, J. Acoust. Soc. Am. **146**, 742 (2019).
[18] J. W. McIver, B. Schulte, F.-U. Stein, T. Matsuyama, G. Jotzu, G. Meier, and A. Cavalleri, Light-induced anomalous Hall effect in graphene, Nat. Phys. **16**, 38 (2020).
[19] M. S. Rudner, N. H. Lindner, E. Berg, and M. Levin, Anomalous Edge States and the Bulk-Edge Correspondence for Periodically Driven Two-Dimensional Systems, Phys. Rev. X **3**, 031005 (2013).
[20] F. Nathan and M. S. Rudner, Topological singularities and the general classification of Floquet–Bloch systems, New J. Phys. **17**, 125014 (2015).
[21] W. Zhu, Y. D. Chong, and J. Gong, Floquet higher-order topological insulator in a periodically driven bipartite lattice, Phys. Rev. B **103**, L041402 (2021).
[22] R. W. Bomantara, Z_4 parafermion $\pm\pi/2$ modes in an interacting periodically driven superconducting chain, Phys. Rev. B **104**, L121410 (2021).
[23] W. Zhu, H. Xue, J. Gong, Y. Chong, and B. Zhang, Time-periodic corner states from Floquet higher-order topology, Nat. Commun. **13**, 1 (2022).
[24] H. C. Po, L. Fidkowski, T. Morimoto, A. C. Potter, and A. Vishwanath, Chiral Floquet Phases of Many-Body Localized Bosons, Phys. Rev. X **6**, 041070 (2016).
[25] L. Jiang, T. Kitagawa, J. Alicea, A. R. Akhmerov, D. Pekker, G. Refael, J. I. Cirac, E. Demler, M. D. Lukin, and P. Zoller, Majorana Fermions in Equilibrium and in Driven Cold-Atom Quantum Wires, Phys. Rev. Lett. **106**, 220402 (2011).
[26] R. W. Bomantara, Time-induced second-order topological superconductors, Phys. Rev. Res. **2**, 033495 (2020).
[27] R. W. Bomantara and J. Gong, Simulation of Non-Abelian Braiding in Majorana Time Crystals, Phys. Rev. Lett. **120**, 230405 (2018).
[28] R. W. Bomantara and J. Gong, Quantum computation via Floquet topological edge modes, Phys. Rev. B **98**, 165421 (2018).
[29] R. W. Bomantara and J. Gong, Combating quasiparticle poisoning with multiple Majorana fermions in a periodically-driven quantum wire, J. Phys. Condens. Matter **32**, 435301 (2020).
[30] R. W. Bomantara and J. Gong, Measurement-only quantum computation with Floquet Majorana corner modes, Phys. Rev. B **101**, 085401 (2020).
[31] G. J. Sreejith, A. Lazarides, and R. Moessner, Parafermion chain with $2\pi/k$ Floquet edge modes, Phys. Rev. B **94**, 045127 (2016).
[32] A. Hutter and D. Loss, Quantum computing with parafermions, Phys. Rev. B **93**, 125105 (2016).
[33] R. W. Bomantara, Square-root Floquet topological phases and time crystals, Phys. Rev. B **106**, L060305 (2022).
[34] L. Zhou, R. W. Bomantara, and S. Wu, q th-root non-Hermitian Floquet topological insulators, SciPost Phys. **13**, 015 (2022).
[35] P. A. M. Dirac, The quantum theory of the electron, Proc. R. Soc. A **117**, 610 (1928).
[36] O. Klein, Elektrodynamik und wellenmechanik vom standpunkt des korrespondenzprinzips, Z. Phys. **41**, 407 (1927).
[37] W. Gordon, Der comptoneffekt nach der schrödingerschen theorie, Z. Phys. **40**, 117 (1926).
[38] J. Arkinstall, M. H. Teimourpour, L. Feng, R. El-Ganainy, and H. Schomerus, Topological tight-binding models

from nontrivial square roots, Phys. Rev. B **95**, 165109 (2017).
[39] M. Ezawa, Systematic construction of square-root topological insulators and superconductors, Phys. Rev. Res. **2**, 033397 (2020).
[40] G. Pelegrí, A. M. Marques, R. G. Dias, A. J. Daley, V. Ahufinger, and J. Mompart, Topological edge states with ultracold atoms carrying orbital angular momentum in a diamond chain, Phys. Rev. A **99**, 023612 (2019).
[41] W. Ding, Y.-Y. Wang, S.-F. Gao, M.-L. Wang, and P. Wang, Recent progress in low-loss hollow-core anti-resonant fibers and their applications, IEEE J. Sel. Top. Quantum Electron. **26**, 1 (2019).
[42] T. Mizoguchi, Y. Kuno, and Y. Hatsugai, Square-root higher-order topological insulator on a decorated honeycomb lattice, Phys. Rev. A **102**, 033527 (2020).
[43] A. M. Marques, L. Madail, and R. G. Dias, One-dimensional 2^n-root topological insulators and superconductors, Phys. Rev. B **103**, 235425 (2021).
[44] Z. Lin, S. Ke, X. Zhu, and X. Li, Square-root non-Bloch topological insulators in non-Hermitian ring resonators, Opt. Express **29**, 8462 (2021).
[45] A. M. Marques and R. G. Dias, 2^n-root weak, Chern, and higher-order topological insulators, and 2^n-root topological semimetals, Phys. Rev. B **104**, 165410 (2021).
[46] T. Yoshida, T. Mizoguchi, Y. Kuno, and Y. Hatsugai, Square-root topological phase with time-reversal and particle-hole symmetry, Phys. Rev. B **103**, 235130 (2021).
[47] T. Mizoguchi, T. Yoshida, and Y. Hatsugai, Square-root topological semimetals, Phys. Rev. B **103**, 045136 (2021).
[48] R. G. Dias and A. M. Marques, Matryoshka approach to sine-cosine topological models, Phys. Rev. B **103**, 245112 (2021).
[49] L. Song, H. Yang, Y. Cao, and P. Yan, Square-root higher-order Weyl semimetals, Nat. Commun. **13**, 5601 (2022).
[50] D. Matsumoto, T. Mizoguchi, and Y. Hatsugai, Higher-order topological insulator on a martini lattice and its square root descendant, arXiv:2207.14540.
[51] Z.-G. Geng, Y.-G. Peng, H. Lv, Z. Xiong, Z. Chen, and X.-F. Zhu, Square-root-like higher-order topological states in three-dimensional sonic crystals, J. Phys. Condens. Matter **34**, 104001 (2022).
[52] R.-L. Zhang, Q.-P. Wu, M.-R. Liu, X.-B. Xiao, and Z.-F. Liu, Complex–real transformation of eigenenergies and topological edge states in square-root non-Hermitian topolectrical circuits, Ann. Phys. (Berlin) **534**, 2100497 (2022).
[53] M. Kremer, I. Petrides, E. Meyer, M. Heinrich, O. Zilberberg, and A. Szameit, A square-root topological insulator with non-quantized indices realized with photonic Aharonov-Bohm cages, Nat. Commun. **11**, 1 (2020).
[54] M. Yan, X. Huang, L. Luo, J. Lu, W. Deng, and Z. Liu, Acoustic square-root topological states, Phys. Rev. B **102**, 180102(R) (2020).
[55] W. Yan, D. Song, S. Xia, J. Xie, L. Tang, J. Xu, and Z. Chen, Realization of second-order photonic square-root topological insulators, ACS Photonics **8**, 3308 (2021).
[56] L. Song, H. Yang, Y. Cao, and P. Yan, Realization of the square-root higher-order topological insulator in electric circuits, Nano Lett. **20**, 7566 (2020).
[57] See Supplemental Material at http://link.aps.org/supplemental/10.1103/PhysRevLett.129.254301 for the calculation of the phase diagram, topological edge modes, details of the structure design, and discussion about $\pi/3$ and $2\pi/3$ quasienergy edge modes, which also includes Refs. [58,59].
[58] J. K. Asbóth, B. Tarasinski, and P. Delplace, Chiral symmetry and bulk-boundary correspondence in periodically driven one-dimensional systems, Phys. Rev. B **90**, 125143 (2014).
[59] G. H. Wannier, The structure of electronic excitation levels in insulating crystals, Phys. Rev. **52**, 191 (1937).
[60] J. K. Asbóth, Symmetries, topological phases, and bound states in the one-dimensional quantum walk, Phys. Rev. B **86**, 195414 (2012).
[61] J. K. Asbóth and H. Obuse, Bulk-boundary correspondence for chiral symmetric quantum walks, Phys. Rev. B **88**, 121406(R) (2013).
[62] A. M. Marques and R. G. Dias, One-dimensional topological insulators with noncentered inversion symmetry axis, Phys. Rev. B **100**, 041104(R) (2019).
[63] J. Tervo and J. Turunen, Paraxial-domain diffractive elements with 100% efficiency based on polarization gratings, Opt. Lett. **25**, 785 (2000).
[64] M. A. Bandres and M. Guizar-Sicairos, Paraxial group, Opt. Lett. **34**, 13 (2009).
[65] A. Carnicer, I. Juvells, D. Maluenda, R. Martínez-Herrero, and P. M. Mejías, On the longitudinal component of paraxial fields, Eur. J. Phys. **33**, 1235 (2012).
[66] C. Moodley, H. Sroor, V. Rodríguez-Fajardo, Q. Zhan, and A. Forbes, Demonstrating a modal approach to paraxial light propagation for photonics education, in *Education and Training in Optics & Photonics Conference*, edited by A. Danner, A. Poulin-Girard, and N. Wong (Optica Publishing Group, Washington, DC, 2021), p. W2A.6.
[67] Z.-G. Chen, R.-Y. Zhang, C. T. Chan, and G. Ma, Classical non-Abelian braiding of acoustic modes, Nat. Phys. **18**, 179 (2022).